Additive Manufacturing of Bovine Serum Albumin-based Hydrogels and Bioplastics

*Patrick T. Smith,[†] Benjaporn Narupai,[†] Jonathan H. Tsui,[‡] S. Cem Millik,[†] Ryan T. Shafranek,[†] Deok-Ho Kim,[‡] Alshakim Nelson[†]**

[†]Department of Chemistry, University of Washington, Seattle

[‡]Department of Bioengineering, University of Washington, Seattle

ABSTRACT

Bio-sourced and biodegradable polymers for additive manufacturing could enable the rapid fabrication of parts for a broad spectrum of applications ranging from healthcare to aerospace. However, a limited number of these materials are suitable for vat photopolymerization processes. Herein, we report a two-step additive manufacturing process to fabricate robust protein-based constructs using a commercially available laser-based SLA printer. Methacrylated bovine serum albumin (MA-BSA) was synthesized and formulated into aqueous resins that were used to print complex 3D objects with a resolution comparable to a commercially available resin. The MA-BSA resins were characterized by rheometry to determine the viscosity and the cure rate, as both of these parameters can ultimately be used to predict the printability of the resin. In the first step of patterning these materials, the MA-BSA resin was 3D printed, and in the second step, the printed construct was thermally cured to denature the globular protein and increase the intermolecular noncovalent interactions. Thus, the final 3D printed part was comprised of both chemical and physical cross-links. Compression studies of hydrated and dehydrated constructs demonstrated a broad range of compressive strengths and Young's moduli that could be further modulated by adjusting the type and amount of co-monomer. The printed hydrogel constructs demonstrated good cell viability (> 95%) after a 21-day culture period. These MA-BSA resins are expected to be compatible with other vat photopolymerization techniques including digital light projection (DLP) and continuous liquid interface production (CLIP).

INTRODUCTION

Bio-sourced materials that can replace existing petroleum-based materials are essential for sustainability. Moreover, bio-sourced materials with greater functionality will be required to meet the demands for the full spectrum of applications from aerospace to medicine. Additive manufacturing (AM) is an advanced fabrication method for creating complex 3D geometries and shows great promise for the future of manufacturing.[1,2] While many forms of AM exist, vat photopolymerization methods are advantageous for the speed at which high resolution objects can be produced.[3,4] Laser-based stereolithography (SLA) 3D printing is a form of vat photopolymerization wherein a laser is scanned through photocurable resin to selectively cure the growing feature. This method of 3D printing provides micron-scale features with good accuracy and reproducibility.[5] While this technique enables access to high resolution 3D geometries, it is greatly limited by the availability of resins designed for additive processes.[6,7]

There have been few examples of bio-sourced materials that were designed for AM via a vat photopolymerization process.[8–12] Ideally, these materials should also be biodegradable to create a closed loop cycle. Other biodegradable resins have been reported, such as poly(alkyl fumarate) derivatives[13–15] and poly(lactide).[16] One of the main challenges in designing new oligomeric and polymeric resins for SLA is the increased viscosity of the resin, based on concentration and molecular weight as predicted by the Mark-Houwink equation.[17] Resins with high viscosity do not adequately self-level and recoat the surface of the resin tray between layers, resulting in long print times or unsuccessful prints.[18–20] An alternative design strategy is to employ cyclic, branched, or dendritic polymer architectures, or cross-linked unimolecular particles, that have a lower intrinsic viscosity relative to a linear polymer of comparable molecular weight.[21,22]

In this report, we demonstrate a protein-based resin for vat photopolymerization using bovine serum albumin (BSA) that can be utilized to 3D print objects with complex geometries. BSA is a water-soluble, globular protein that is relatively abundant and low-cost. A critical aspect of this protein is that it is a single polypeptide chain that is folded into a globular particle. Despite the high molecular weight of BSA, ~66.5 *k*Da, the protein has an extremely high solubility in water (up to ~40 % w/v) due to its globular shape. The protein is comprised of 68% α-helical structure and contains 17 disulfide bonds, with a net negatively charged surface that helps the protein resist aggregation.[23,24] BSA is particularly advantageous over gelatin as a protein scaffold because it does not self-assemble or aggregate as its concentration in aqueous solution is increased. For example, at concentrations above ~2 wt%, the Gel-MA resin forms a gel, which limits its printability in a vat photopolymerization process.[25]

We developed a two-step process for 3D printing methacrylated BSA (MA-BSA), where in the first step, the protein is photo-patterned 3D dimensionally, and in a separate subsequent step, the protein is denatured during a thermal curing step to improve the mechanical properties of the printed construct (**Figure 1**). The resolution capabilities of the MA-BSA resin, using a commercially available Form2 printer, were comparable to a commercially available resin (~200 μm), and 3D objects with complex lattice geometries were fabricated. The dual cross-linked network, comprised of chemical cross-links from the printing step and physical cross-links from the thermal curing step, afforded printed hydrogels and bioplastics with excellent mechanical properties. The resulting hydrogels and bioplastics are suitable for stiff structural elements and were biocompatible and biodegradable.

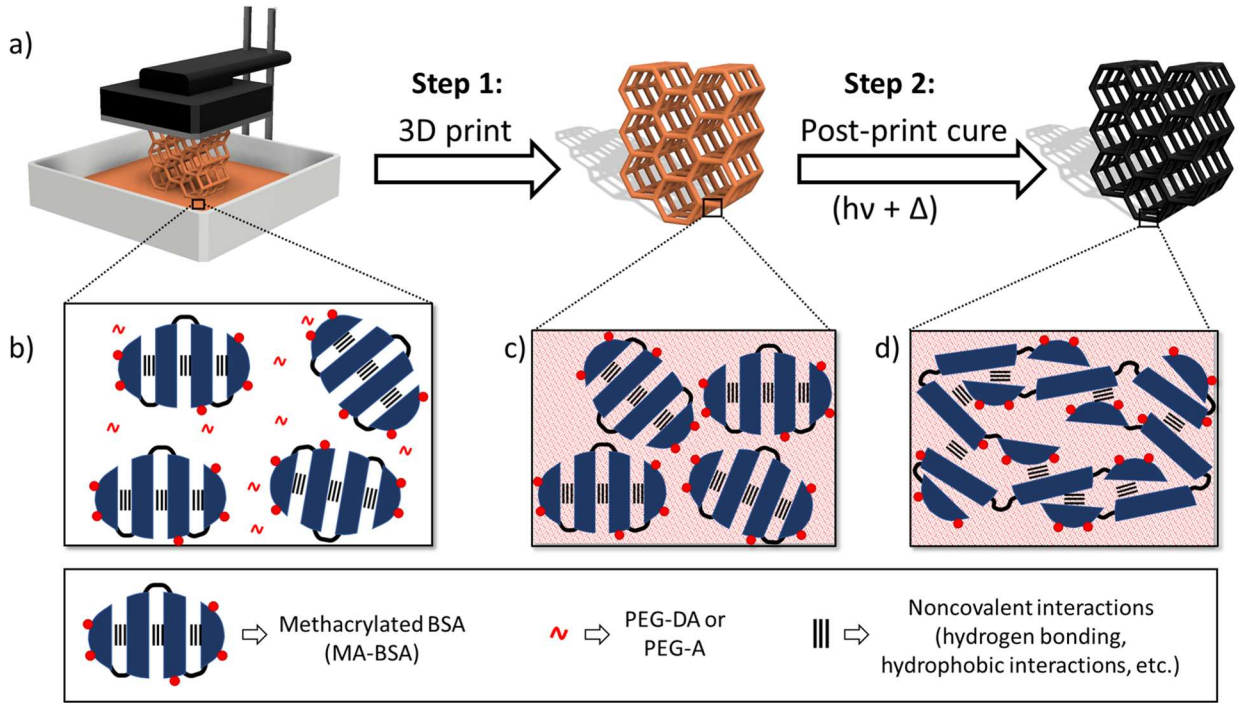

Figure 1. Graphical overview of the two-step process to fabricate protein-based hydrogels and bioplastics using vat photopolymerization. (a) This idealized general scheme as shown involved a resin comprising (b) a solution of highly aqueous-soluble MA-BSA that was initially polymerized via photo-initiated free radical polymerization to afford a 3D printed construct. (c) The polymerized protein network was then cured by first irradiating with 400 nm light to induce further polymerization of any unreacted components, and then heat treated (120 °C) for 3 h to afford (d) a denatured protein matrix which improves the mechanical properties of the printed construct.

EXPERIMENTAL SECTION

Materials. All materials were purchased from Sigma Aldrich unless otherwise stated. Methacrylic anhydride (94%), Tris(2,2′-bipyridyl)dichlororuthenium(II) hexahydrate ($Ru(bpy)_3Cl$) (99.95%), poly(ethylene glycol) diacrylate (M_n 700 Da), poly(ethylene glycol) methyl ether acrylate (M_n 480 Da) and sodium persulfate (SPS) were used as received. Ultra-pure and ultra-low fatty acid content BSA was purchased from Nova Biologics. Formlabs Standard Clear Resin (FLGPCL04) was purchased from Formlabs.

Methacrylation of BSA. A procedure for methacrylation of gelatin was modified and used to methacrylate BSA.[26] In short, BSA (20 g, 0.3 mmol) and $NaHCO_3$ / Na_2CO_3 buffer (200 mL, 0.25 M, pH 9.0) were added to a 1000 mL round-bottom flask equipped with a magnetic stir bar. The mixture was stirred in an ice bath until the BSA dissolved completely. Then, methacrylic anhydride (4 mL, 27 mmol, ~2.5 eq. per lysine residue) was added dropwise to the BSA solution over 10 min. The reaction mixture was stirred in an ice bath for 1 h. The crude product was diluted and dialyzed against deionized (DI) water for 48 h. After lyophilization, the product was isolated as a white powder of MA-BSA (18.3 g, 91.5 % yield). The percent functionalization of the available lysines of BSA with methacryloyl functionalities was determined using a 2,4,6-trinitrobenzene sulfonate (TNBS) assay.[27] The TNBS assay is a method used to quantify primary

amino groups by *N*-trinitrophenylation of primary amines, which have high absorption at 335 nm. BSA and MA-BSA were dissolved in carbonate-bicarbonate buffer at a concentration of 20 µg/mL. A 0.01% (w/v) solution of TNBS (0.25 mL) was added to 0.5 mL of each protein solution. The samples were incubated at 37 °C for 2 h. To quench the reaction, 0.25 mL of 10% SDS and 0.125 mL of 1 N HCl were added to each sample. The absorption of each solution was measured at 335 nm with a UV/VIS spectrophotometer (Agilent 8453, **Figure S1**). The absorbance of the MA-BSA was compared to the absorbance of native BSA and the percent functionalization was then calculated as follows:

$$\%\ functionalization = \frac{Abs_{BSA} - Abs_{MABSA}}{Abs_{BSA}}\ x\ 100$$

Characterization of secondary structure. Circular dichroism (CD) spectroscopy (Jasco J-720 spectropolarimeter) was used to evaluate the structure of BSA in solution after methacrylation. The experiments were performed at 25 °C in 1 mm quartz cuvettes. The wavelength of the CD spectrum was measured from 190 to 270 nm, with a step resolution of 0.2 nm, a scanning rate of 100 nm/min, a 1 s response time, and 2.0 nm bandwidth. The spectrum displayed for native BSA and MA-BSA were an average of 8 spectra (**Figure S2**). Solvent-corrected CD spectra were analyzed using the BeSTSel web server (http://bestsel.elte.hu) to estimate the secondary structure.[28,29]

Preparation of MA-BSA based resin for vat photopolymerization. All resin formulations were prepared in amber bottles and covered in aluminum foil to prevent auto-polymerization. The weight percentages are based on the total composition of the resin, including the aqueous solvent. As a representative example, we describe here the preparation of the resin with 30 wt% MA-BSA and 5 wt% poly(ethylene glycol) diacrylate (PEG-DA). First, 0.3 g of PEG-DA was dissolved in 3.66 mL of DI water, then 1.8 g of MA-BSA was slowly added to this solution with gentle mixing until dissolved. Next, 0.075 wt% $Ru(bpy)_3Cl$ dissolved in 120 µL of DI water and 0.24 wt% SPS dissolved in 120 µL of DI water were sequentially dissolved into the resin formulation. The final resin formulation was covered in aluminum foil and stored at 4 °C until use. To prepare other formulations, the same procedure was followed, changing only the co-monomer and DI water quantities.

Fabrication of MA-BSA hydrogels using SLA printing. A Formlabs Form 2 printer was used to fabricate the hydrogel constructs. The build plate and resin tray were modified to reduce the total volume of resin required to print. The build plate was cut down to 45 mm x 45 mm and a 48 mm x 78 mm x 28 mm border was 3D printed on a Flashforge® Creator Pro, then glued to the resin tray to form a small reservoir within the standard resin tray. 3D constructs were designed with Autodesk® Fusion 360 or downloaded from Thingiverse®. The resin was poured within the border and ice was placed around the outside of the border to prevent the temperature of the resin from increasing during printing. Hydrogel constructs were then printed in 'open mode' with a layer height of 50 µm. Upon completion of the print, samples were removed from the build plate, rinsed in DI water to remove any uncured resin, and post cured in a custom photo-curing chamber (Quans, 400 nm, 1 mW/cm^2) for 90 min. Some samples were further thermally cured. These samples were air-dried after the photo-curing step, then placed in the 120 °C oven for 180 min.

Swelling experiments. 3D printed cylindrical disks (10 mm diameter x 5 mm height) were used for mass loss and swelling experiments. After printing and post-photo curing, the disks were

lyophilized to obtain the initial dry weight ($m_{dry,i}$). Samples were then submerged in an excess of DI water and weighed after 1 day ($m_{swollen}$). The swollen samples were then freeze-dried and weighed again (m_{dry}). The swelling ratio (q) and mass loss were calculated as follows:

$$\%\ mass\ loss = \left(\frac{m_{dry,i} - m_{dry}}{m_{dry,i}}\right) \times\ 100\%$$

$$q = \frac{m_{swollen}}{m_{dry}}$$

Rheological characterization. Rheological characterization was performed on a TA Instruments Discovery Hybrid Rheometer-2. Viscosity versus shear rate experiments were performed at a shear rate increasing from 1-100 s^{-1} using a 40mm cone and plate geometry with a cone angle of 1.019°, a solvent trap, and a gap height of 26 μm. Due to surface tension effects, only the range from 6-100 Pa·s was reported.[30] To conduct photo-rheology experiments, the rheometer was outfitted with a collimated light source (λ = 400 nm, 10 mW cm^{-2}, Thorlabs) that was turned on 60 seconds after the start of the experiment. Using a 20 mm parallel plate and a gap height of 1000 μm, the storage and loss moduli were monitored for a total of 150 seconds at 1% strain and 6.28 rad/s.

Uniaxial compression testing. Compression testing was performed using an Instron 5585H load frame with a 2 *k*N and 50 *k*N load cell for hydrated and dehydrated samples, respectively. Cylindrical compression samples (10 mm diameter x 5mm height) were 3D printed as described above. Samples were tested both in their dehydrated state and at equilibrium swelling with DI water. Thermally treated samples were air dried after photo-curing, placed in a 120 °C oven for 180 min, then tested either in their dehydrated state or at equilibrium swelling. All tests were conducted at room temperature (22 °C) using a crosshead rate of 1.3 mm/min until specimen failure or 80% strain. Prior to testing, the hydrated samples were removed from the DI water and blotted dry with a Kim wipe. Then, the dimensions of each specimen were measured with calipers. At least 5 specimens of each formulation were tested. The modulus, compressive strength, and toughness were determined from the resulting stress-strain curve. The toughness was determined by calculating the area under the stress-strain curves using Matlab. The compressive modulus was determined from the slope of the elastic region of the stress-strain curve.

Scanning electron microscopy. Scanning electron microscopy (SEM) samples were air dried after printing and imaged using an Apreo-S SEM operated at 2.0 *k*V.

Print resolution and accuracy. The accuracy and resolution of the MA-BSA resin was compared with the commercial Form 2 resin by printing test structures with various sized features. The test structure was designed to have hollow squares that increase in size from 400 μm to 2000 μm and posts that range from 100 μm to 1000 μm. The dimensions of the printed features were measured using Image J and compared to the CAD dimensions (**Figure 3 and S9**).

Cell culture and biocompatibility assessment: Hydrogel films 1 mm thick and 5 mm in diameter were inserted into wells of a poly(styrene) 96-well culture plate. NIH/3T3 murine fibroblasts (ATCC, VA, USA) were then seeded onto these thin films at a density of 1 x 10^5 cells/cm^2 and cultured in high-glucose Dulbecco's Modified Eagle Medium (DMEM) (Invitrogen, MA, USA) supplemented with 10% fetal bovine serum and 1% penicillin-streptomycin (Invitrogen). Cultures were maintained for 21 days before cells were stained with a live/dead

viability kit (Invitrogen) following the protocol provided by the manufacturer. Stained samples were then imaged using a widefield fluorescent microscope (A1R, Nikon Instruments, NY, USA) at 20 x magnification. Live cells appeared green (calcein-AM excitation/emission: 488/515 nm), while dead cells appeared red (ethidium homodimer-1 excitation/emission: 570/602 nm). Analysis of the images was conducted using ImageJ image processing software (National Institutes of Health, MD, USA).

Enzymatic degradation of printed constructs. For the *in vitro* degradation study, hexagonal lattice structures were printed using formulation 4 (**Table 1**) and degraded using proteinase K. The lattice structures were initially weighed, then incubated at 37 °C in either Tris-$CaCl_2$ buffer (pH 8 0.1 M, GoldBio) with a final proteinase K concentration of 2 mg/mL, or the Tris-$CaCl_2$ buffer alone as a control. Every 24 hours, the lattices were removed from solution, blotted dry with a Kim wipe, weighed, then placed into a fresh solution of enzyme or buffer. Optical images were taken at different time points.

RESULTS AND DISCUSSION

Radical photopolymerization of acrylates and methacrylates is a common reaction scheme employed in the development of resins for vat photopolymerization.[4,31–37] The polymerization occurs rapidly, and the incorporation of multiple (meth)acrylates per molecule decreases the time to reach gel-point. We note that during the 3D printing step, we did not seek to fully cure the structure as it was printed. Instead, the printed construct was sufficiently cross-linked to hold its form, and a post-print curing step ($h\nu$ and thermal) was necessary to further improve the mechanical properties of the material.

Commercially available BSA was converted into MA-BSA by reaction with methacrylic anhydride in an aqueous buffer. Based on a TNBS assay, we determined that >90% of the available lysines were converted into methacrylamides. We hypothesized that MA-BSA would make an excellent cross-linker and resin component based on the presence of multiple (ca. 27-31) methacrylamides present on the protein surface.[38] The MA-BSA was soluble in aqueous solutions at concentrations up to 40 wt%.

Circular dichroism (CD) spectroscopy was employed to assess whether the protein underwent significant changes in terms of its secondary conformation upon methacrylation. The CD spectra for the functionalized and unfunctionalized BSA were deconvoluted using BeStSel to estimate each protein's secondary structure. The BeStSel program produced similar values for both native and methacrylated BSA (**Table S1**), which suggests that there was not a significant change in the overall secondary structure of the BSA after methacrylation.

The viscosity and the rate of photo-curing of MA-BSA formulations (**Table 1**) were evaluated via rheometry and optimized for vat photopolymerization. Resins that have a high viscosity (>10 Pa·s)[39,40] are slow to self-level and exert greater capillary forces that hamper vat photopolymerization. MA-BSA formulations over the range of 10-40 wt% in aqueous solution were investigated (**Figure 2a)**. Formulations up to 30 wt% MA-BSA maintained a low viscosity up to 0.035 Pa·s, with a more significant increase in the viscosity for 35 wt% and 40 wt% MA-BSA (1.56 Pa·s and 29.4 Pa·s, respectively). Based on these results, we formulated resins with 30 wt% and 35 wt% MA-BSA with the goal of maximizing protein content while maintaining a viscosity below 10 Pa·s.

The dwell time and intensity of the laser (405 nm) on the Form 2 printer are not adjustable, and thus, the photo-curing rate of the resin formulation must be optimized for the printer. The cure rates of the MA-BSA formulations were investigated by photo-rheology using a 400 nm light source and were compared to the resin available from the commercial supplier (**Figure S4**). Ruthenium tris(bipyridyl) chloride ($Ru(bpy)_3Cl$) and sodium persulfate (SPS) were used as the photo-initiating system for their excellent solubility in water and high molar extinction coefficient at 405 nm.[10,12] We observed that formulations comprising MA-BSA (30 wt%), $Ru(bpy)_3Cl$ (0.075 wt%) and SPS (0.24 wt%) did not cure at a rate appropriate for SLA printing (**Figure S5**). In this case, nearly 30 s passed before an appreciable change in the storage modulus (G') occurred. This may be attributed to the large size of BSA (~66 *k*Da) and limited number of methacrylamides available to form a cross-linked network. Based on these experiments, we hypothesized that the addition of a second reactive monomer could increase the cure rate of the resins. Thus, poly(ethylene glycol) diacrylate (PEG-DA, M_n 700 Da) or poly(ethylene glycol) methyl ether acrylate (PEG-A, M_n 480 Da) were included as additives in the formulations.

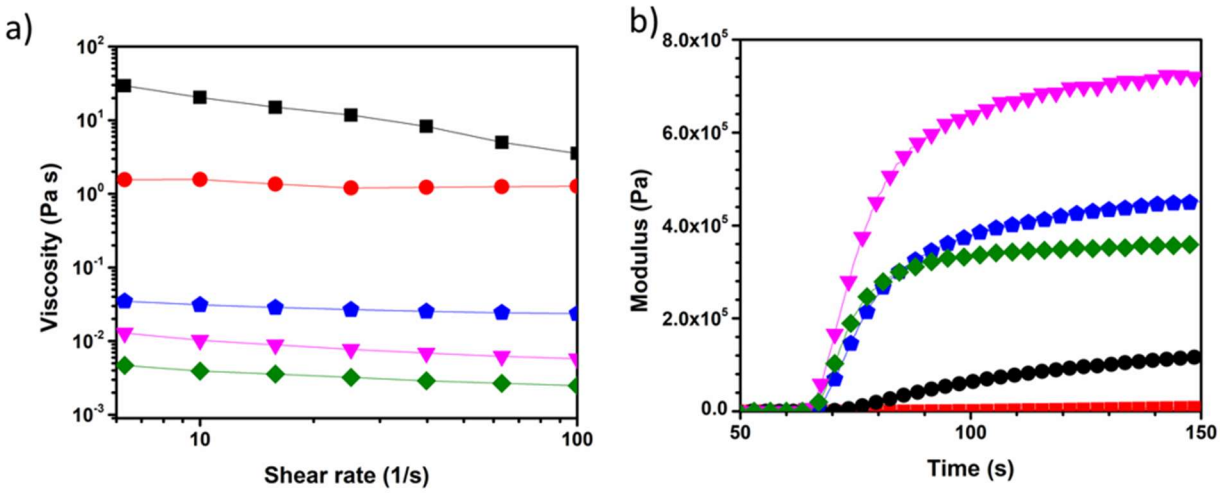

Figure 2. Rheometrical evaluation of MA-BSA formulations to determine viscosity and rate of photo-curing. (a) Viscosity versus shear rate data for 10-40 wt% MA-BSA formulations; 40 wt% MA-BSA (black squares), 35 wt% MA-BSA (red circles), 30 wt% MA-BSA (blue pentagons), 20 wt% MA-BSA (pink triangles), 10 wt% MA-BSA (green diamonds). (b) Photo-rheology of 30 wt% MA-BSA resin with various amounts of co-monomer. The light source (400nm) was turned on after 60 s; no co-monomer (red squares), 1 wt% PEG-DA (black circles), 5 wt% PEG-DA (blue pentagons), 10 wt% PEG-DA (pink triangles), 10 wt% PEG-A (green diamonds).

The time required to reach gel point ($G' = G''$) and the cure rate (based on the change in G' upon irradiation with 400 nm light) were used to assess the formulations for suitability in vat photopolymerization.[41,42] We first evaluated the time to reach gel points because it has been previously reported that the macromer conversion at the interface between layers should be slightly higher than the gel point to ensure chemical bonding between layers.[43] Additionally, a successful SLA resin should surpass its gel point quickly. The 30 wt% MA-BSA formulation without any additives required 18 s of irradiation to reach its gel point. The addition of a co-monomer into the

formulation decreased the required irradiation time to 5.5 s, 4.0 s, and 2.2 s for 1 wt%, 5 wt%, 10 wt% PEG-DA, respectively. The mono-functional co-monomer, PEG-A, also decreased the time to reach gel point (3.2 s) relative to the MA-BSA formulation at 30 wt%. The cure rate based on the change in G' over time was assessed for each of the formulations over the first 30 s of irradiation (**Table 1**). The storage modulus of the formulation without any co-monomer increased at a rate of 0.006 *k*Pa/s while the incorporation of monomer increased the cure rate by orders of magnitude (three orders of magnitude for 1 wt% and four orders of magnitude of Pa/s for both 5 and 10 wt% added co-monomer). Importantly, the addition of co-monomer does not significantly alter the viscosity, and the resin remains well within the working range for SLA printing (**Figure S6**).

All of the formulations were evaluated using a Form2 printer. The 30 wt% MA-BSA formulations with the inclusion of 5-10 wt% additive (**Table 1**, entries 3-5) were the best candidates as resins, which was consistent with our rheological experiments. The resin formulation with 1 wt% co-monomer (**Table 1**, entry 1) printed the initial 10-20 layers before the printed part delaminated from the build plate. The formulations with 35 wt% MA-BSA were also unacceptable as resins because they were too viscous. Based on these results, the successful formulations met two requirements: (i) a resin viscosity that was <3.4 Pa·s, and (ii) a cure rate that was ≥13.5 *k*Pa/s.

Table 1. Rheometrical data for MA-BSA resin formulations.

Entry	wt % MA-BSA	Comonomer (wt%)	Printable	Viscosity (Pa s)	Gel point (s)	G′ rate of change[a] (kPa/s)
1	30	--	No	0.035	18	0.006
2	30	PEG-DA (1)	No	0.020	5.5	1.61
3	30	PEG-DA (5)	Yes	0.061	4.0	14.0
4	30	PEG-DA (10)	Yes	0.267	2.2	24.2
5	30	PEG-A (10)	Yes	0.072	3.2	13.5
6	35	PEG-DA (5)	No	8.2	4.5	19.1
7	35	PEG-DA (10)	No	3.4	4.8	50.1

[a] Based on the first 30 s of irradiation.

The resolution of each print is governed by both the printer (laser spot size and laser accuracy) and the curing kinetics of the resin. We designed a CAD file for a test structure with an array of fins (100 – 1000 μm), as well as an array of square holes with widths that ranged from 400 – 2000 μm. This test structure (**Figure 3**) was used to evaluate the resolution limit of the formulation with the highest printable MA-BSA content (**Table 1**, entry 4). The smallest fin printed was 243 μm and the smallest square hole resolved was 700 μm. In comparison, the smallest feature fin and hole for a commercially available acrylate resin was 173 μm and 400 μm, respectively. In general, the printed constructs were consistent with the CAD model, and on average, the MA-BSA printed structure deviated higher (67.5 μm) than the dimensions designed in the CAD model. The commercially available resin exhibited a similar behavior but with a smaller deviation from the CAD model (8.9 μm).

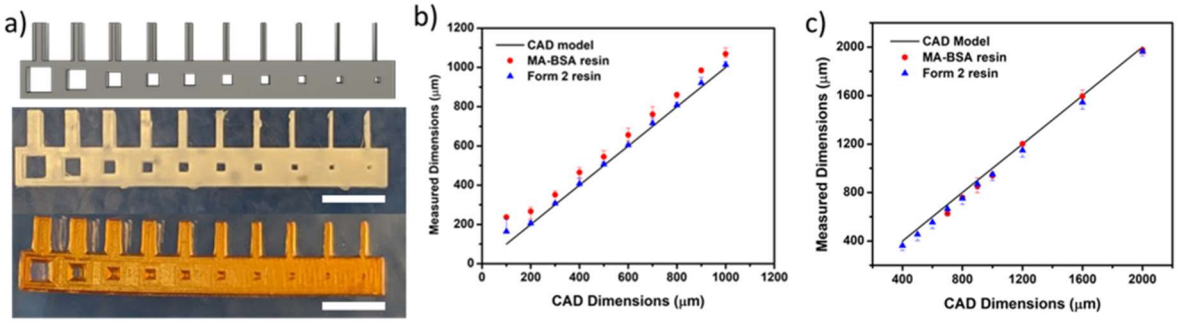

Figure 3. A test structure comprised of lines/spaces of varying line widths from (100 μm to 1000 μm) and square holes with dimensions from (400 μm to 2000 μm) was designed and printed using the Form2 printer. (a) Comparison of the original CAD, printed commercial resin, and formulation with 30 wt % MA-BSA and 10 wt % PEG-DA (top to bottom, scale bar 5mm). Plots showing the measured feature sizes for the printed (b) lines and (c) square holes versus the CAD.

The as-printed structures of the MA-BSA formulation were hydrogels with a water content of ca. 60 wt%. These structures were subjected to a post-print curing step to induce further cross-linking within the material. The printed hydrogel samples were first irradiated with 400 nm light for 1.5 h to further polymerize any unreacted meth(acrylate)s. Then, the samples were dehydrated and thermally cured at 120 °C for 180 min. During this step, the BSA protein was also expected to denature, which would increase the physical associations between protein chains via hydrophobic and hydrogen bonding interactions.[44–47] The printed and cured samples afforded bioplastics that could be re-hydrated with water to re-form the hydrogel. Swelling studies were performed to determine the amount of water the printed constructs absorbed (swelling ratio, q) and the gel fraction for the material (based on percent mass loss) for each formulation after printing (**Table S2**). The thermally cured samples exhibited lower swelling ratios and decreased mass loss relative to the non-cured samples. This difference could be attributed to the denaturation of BSA during the thermal curing step, which would lead to an increase in intermolecular interactions between protein chains. As a result, there are more physical associations present within the re-hydrated hydrogel matrix and the swelling ratio decreased.

We also observed that the difunctional monomer, PEG-DA, afforded samples with a lower swelling ratio (2.64) and mass loss after swelling (3.3%) than the monofunctional monomer, PEG-A (3.32 and 9.9 %, respectively). Additionally, the concentration of PEG-DA was inversely related to the swelling ratio as 5 wt % PEG-DA absorbed 81 % more water than 10 wt% PEG-DA. Thus, the reswelling behavior of the MA-BSA hydrogels can be controlled by altering the cross-linking density of the matrix.

The same formulation that was used to print the resolution test structures (**Table 1**, entry 4) was also used to print lattice geometries. These examples demonstrate the successful printing of complex geometries with good resolution (250 μm struts) (**Figure 3**). The SEM images of the printed lattices also showed that 50 μm layer heights were clearly visible when angled structures were formed from offset stacked layers (**Figure 3c**).

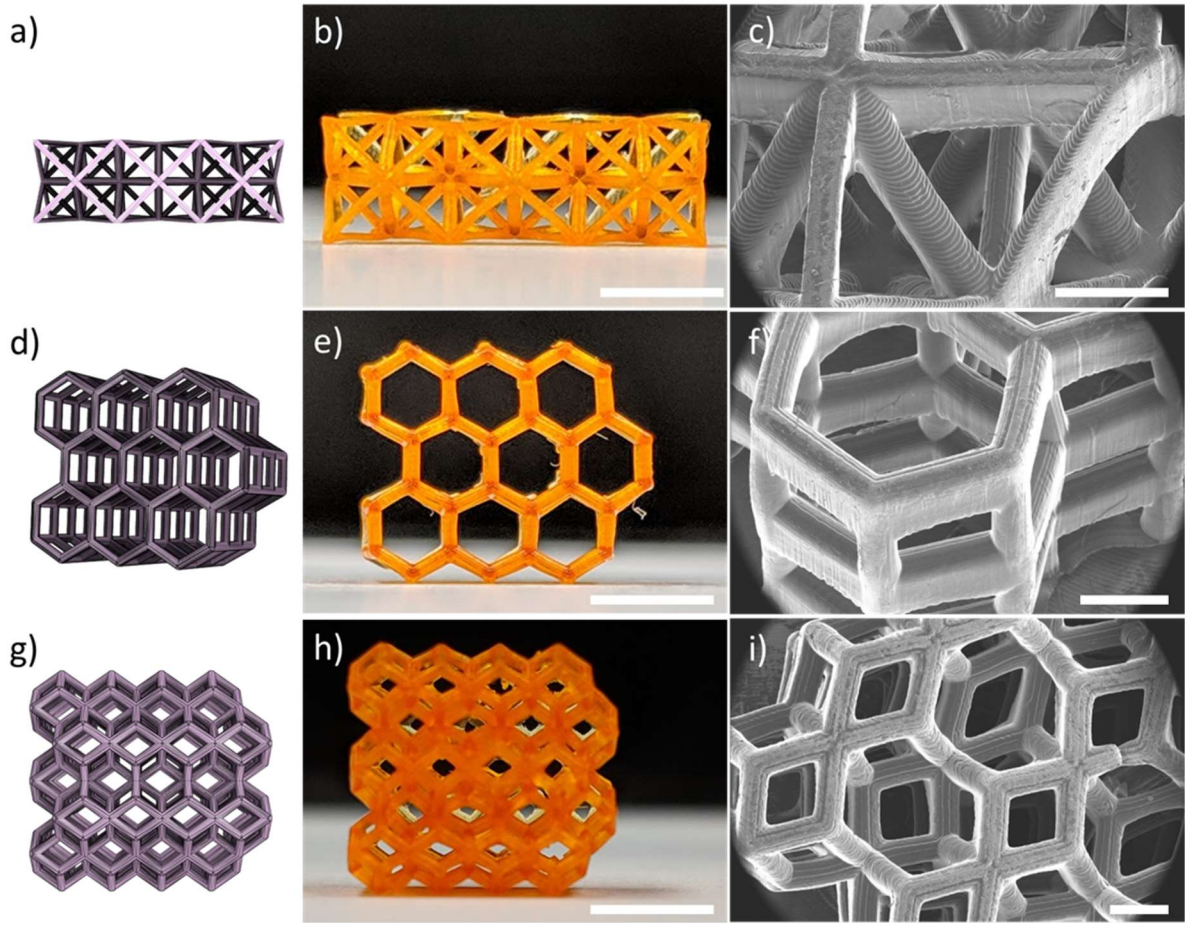

Figure 4. Lattice designs were 3D printed using the formulation comprised of 30 wt % MA-BSA and 10 wt % PEG-DA. The CADs are shown in (a), (d), and (g); optical images are shown in (b), (e), and (h) where the scale bars represent 5 mm; representative SEM images are shown in (c), (f), and (i) where the scale bars represent 1 mm. The samples shown are the dehydrated constructs after the thermal cure.

Uniaxial compression tests were performed to characterize the mechanical properties of cured hydrogels and the corresponding dried bioplastics. The compressive stress-strain curves are plotted

in **Figure 5a-d** and the corresponding data are in **Table S4** and **S5**, where we compared the monofunctional PEG-A versus difunctional PEG-DA as the additive. As expected, the samples with 10 wt% PEG-A had a lower compressive modulus than samples with 10 wt% PEG-DA (3.3 MPa and 6.3 MPa, respectively). This is attributed to the linear chain architecture afforded by PEG-A versus the highly crosslinked network chain architecture that arose from PEG-DA. Samples that were thermally cured exhibited markedly different stress-strain curves compared to un-cured samples. For the hydrated samples (hydrogels), the thermal treatment increased the compressive strength by over 500%, 175%, and 200% for 5 wt% PEG-DA, 10 wt% PEG-DA and 10 wt% PEG-A, respectively. This increase in compressive strength could be the result of the formation of increased noncovalent interactions between the protein chains, forming a dual-crosslinked network. Secondary structural motifs such as intermolecular β-sheets have previously been reported for BSA upon thermal denaturation above 70 °C.[48] The presence of additional intermolecular physical cross-linking was corroborated by the decreased swelling ratio of the thermally cured samples (**Table S2**).

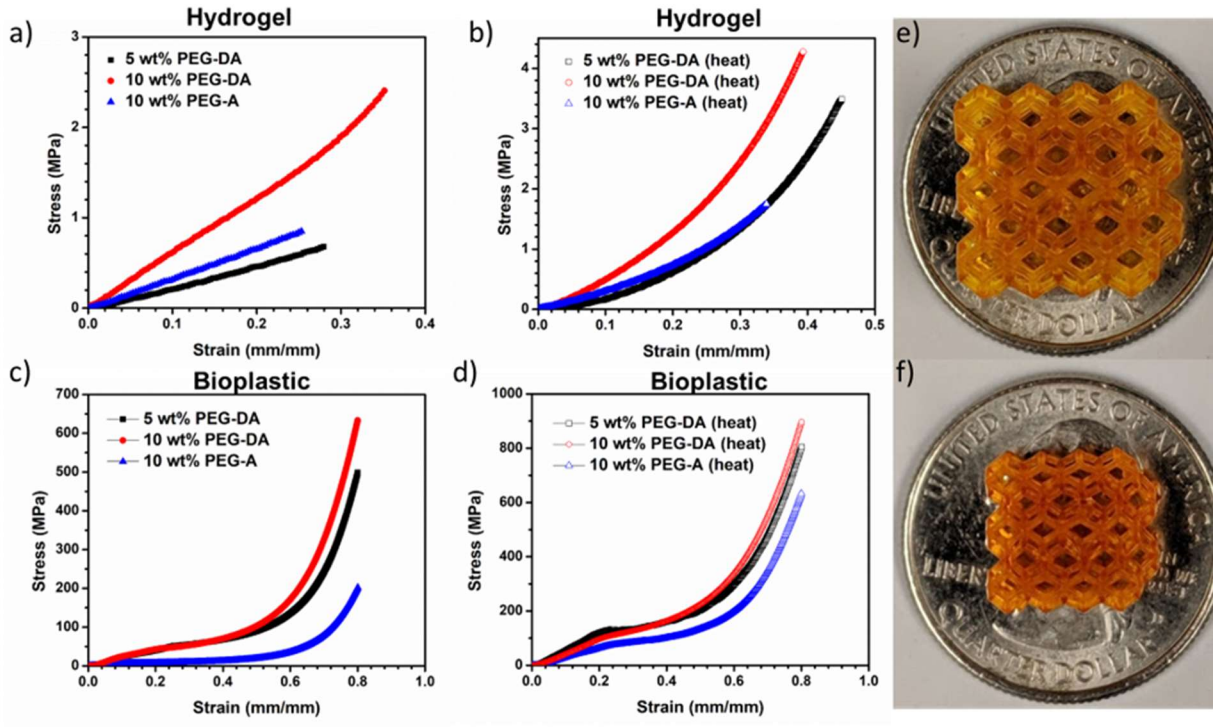

Figure 5. Compressive stress vs strain curves of (a) the 'as printed' hydrogel after equilibrium swelling in water, (b) the thermally cured hydrogel after equilibrium swelling, (c) the 'as printed' sample in the dehydrated state, and (d) the thermally cured sample in the dehydrated state. Photographs of a representative printed lattice are shown in the sample in the (e) swollen hydrogel state and (f) dehydrated state.

Similar to the hydrogels, the bioplastics (**Figure 5c**) with PEG-A additive exhibited a lower modulus than the bioplastics with PEG-DA (73 MPa and 473 MPa, respectively). The thermally cured and dehydrated samples (Figure 5d) also had a much higher modulus than the uncured samples (Figure 5c). For example, the 10 wt% PEG-A bioplastic had a compressive modulus of 73 MPa without the thermal cure and increased to 382 MPa with the thermal cure. Surprisingly,

the thermally cured 5 wt% PEG-DA bioplastic had the highest modulus of all formulations, 638 MPa. We attribute this to the greater proportion of MA-BSA present relative to the total polymer content. The higher concentration of MA-BSA increased the number of inter-protein non-covalent interactions that could occur.

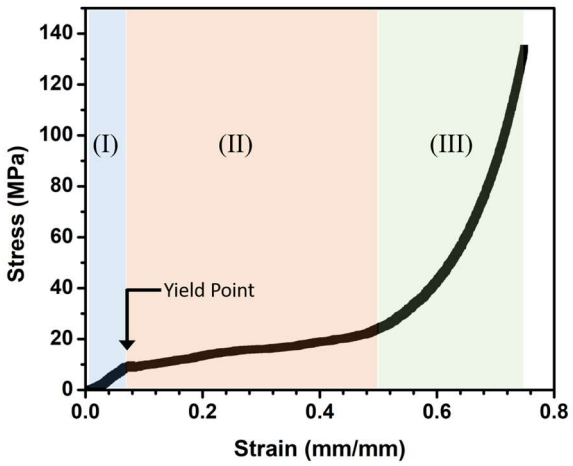

Figure 6. Graph of compressive stress versus strain for a cast dehydrated sample of 30 wt% MA-BSA that has been cross-linked. Three distinct regions were observed and are highlighted: (I) linear elastic region, (II) plateau region, and (III) strain-stiffening region.

Interestingly, the bioplastics that were tested in their dehydrated state did not fail by brittle fracture. Instead, they exhibited plastic deformation and flattened into a disk under compressive load. Figure 6 shows a representative compressive stress versus strain curve for a dehydrated sample of 30 wt% MA-BSA and highlights three distinct regions in the graph. Beyond the linear elastic region, there is a distinct yield point, beyond which plastic deformation occurs. We attribute this behavior to the high molecular weight of the BSA, which can become irreversibly stretched as the load is increased.

Using a fluorescent live/dead assay, the biocompatibility of the MA-BSA formulations with 3T3 fibroblasts was assessed after a 21-day culture period (**Figure 6**). Overall cell viability was good (> 95%), with some hydrogel samples outperforming even conventional tissue-culture plastic. The greatest viability was observed on the 1 wt% PEG-DA hydrogels. While the viability decreased as a function of increasing PEG-DA content, this difference from the 1 wt% formulation was not statistically significant (**Figure 6b**). Interestingly, it also appeared that as PEG-DA content increased, cultured fibroblasts displayed a tendency to form 3D aggregates that formed on top of a layer of adherent cells. This observation could be attributed to a reduction in potential binding sites for cells, because PEG is an anti-fouling and adhesion-resistant material and would induce proliferating cells to preferentially adhere to neighboring cells, rather than to the material surface. Indeed, such behavior has been observed in other PEG-containing hydrogels that have not been

otherwise modified with cell-adhesion ligands.[49–51] While further studies would need to be conducted, particularly with other cell types that do not readily adhere to materials, this property could allow for the use of these hydrogels in applications in which some degree of cell adhesion resistance is desired, such as those that involve contact with flowing blood.

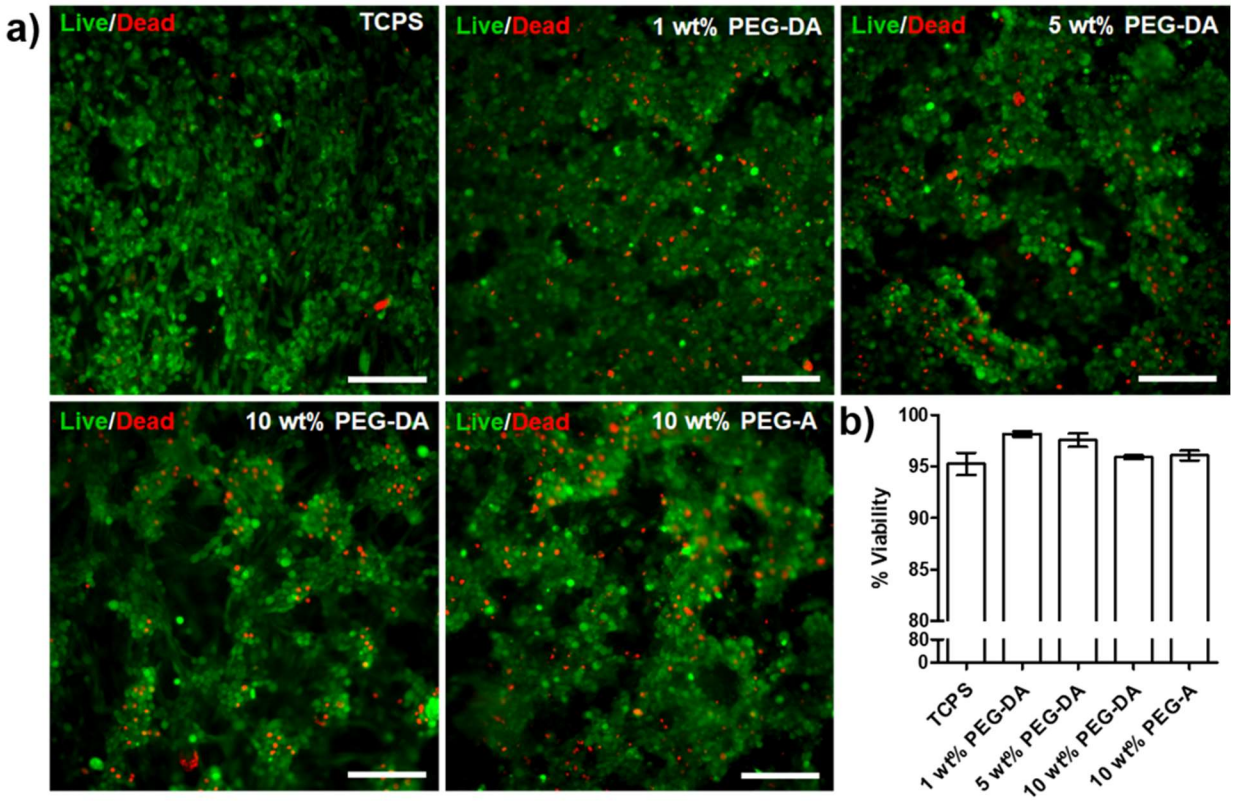

Figure 6. BSA-PEGDA hydrogels are biocompatible with fibroblasts. (a) Representative live/dead staining of fibroblasts on tissue culture polystyrene (TCPS) and on composite hydrogels with varying PEGDA and PEGA content. (b) A high percentage of cells remained viable on hydrogels over a 21-day culture period and viability was comparable to that of TCPS controls.

Finally, the biodegradability of the printed constructs was confirmed by subjecting the printed resin to a protease. The enzymatic degradability of a cross-linked and cured MA-BSA sample (in the absence of any co-monomer) was confirmed by incubating the sample at 37 °C with proteinase K (2 mg/mL). The sample that was cured only with 400 nm irradiation was digested within 2 h, whereas the sample that was irradiated and thermally cured was completely digested within 16 h (**Figure S7**). However, the formulations comprised of MA-BSA and PEG-DA as a co-monomer showed a slower rate of enzymatic degradation. After 1 week of incubation at 37 °C, the irradiated and thermally cured sample degraded and lost 22.0 % of its mass (**Table S3)**. Thus, the addition of the co-monomer significantly reduced the ability of the enzyme to completely degrade the structure. We are currently investigating other cross-linkers that can further enhance or control the degradability of the matrix.

CONCLUSION

In conclusion, we developed a protein-based resin for SLA printing biodegradable hydrogels and bioplastics using a commercial 3D printer. MA-BSA is a versatile platform to create resins on account of its high solubility in water and its low intrinsic viscosity. A two-step procedure was utilized which involved first, patterning the resin using a Form 2 printer, and second thermally curing the printed construct to denature the protein, thus producing a robust 3D structure. The resin was optimized for printability with the inclusion of PEG-DA or PEG-A as a co-monomer. The resin viscosity and rate of photocure were critical parameters that determined the printability of the resin. The formulations that exhibited the best printability had viscosities that were <3.4 Pa·s and a cure rate that was was ≥13.5 kPa/s. The MA-BSA resin formulations performed comparably to a commercially available acrylic resin for the Form 2 printer, with 'as printed' dimensions as small as 230 μm. Upon thermal curing and dehydration, the printed constructs isotropically decreased in size to resolve features down to 170 μm. The printed and thermally cured constructs had excellent mechanical properties for both the reswollen hydrogel and the dehydrated bioplastic (compressive strength of 4.27 MPa at break and 97 MPa at 20% strain, respectively). To the best of our knowledge, this is the first time that a protein's folded and unfolded conformations have been utilized as a switch that facilitates its 3D printing and subsequent physical cross-linking. We expect this strategy to be useful any type of vat photopolymerization process including, digital light projection DLP and continuous layer interface printing (CLIP). These protein-based constructs could be well-suited for load bearing applications in tissue engineering and medical devices.

SUPPORTING INFORMATION

Supporting Information available is available free of charge through the ChemRxiv website. Experimental procedures and characterization data (PDF).

CORRESPONDING AUTHOR INFORMATION

Alshakim Nelson (alshakim@uw.edu)

ACKNOWLEDGEMENTS

This research was supported by the UW Royalty Research Fund.

REFERENCES

(1) Gao, W.; Zhang, Y.; Ramanujan, D.; Ramani, K.; Chen, Y.; Williams, C. B.; Wang, C. C. L.; Shin, Y. C.; Zhang, S.; Zavattieri, P. D. Computer-Aided Design The Status , Challenges , and Future of Additive Manufacturing In. *Comput. Des.* **2015**, *69*, 65–89. DOI: 10.1016/j.cad.2015.04.001.

(2) Shafranek, R. T.; Millik, S. C.; Smith, P. T.; Lee, C.; Boydston, A. J.; Nelson, A. Stimuli-Responsive Materials in Additive Manufacturing. *Prog. Polym. Sci.* **2019**, *93*, 36–67. DOI: 10.1016/j.progpolymsci.2019.03.002.

(3) Appuhamillage, G. A.; Chartrain, N.; Meenakshisundaram, V.; Feller, K. D.; Williams, C. B.; Long, T. E. 110th Anniversary: Vat Photopolymerization-Based Additive Manufacturing: Current Trends and Future Directions in Materials Design. *Ind. Eng. Chem. Res.* **2019**, *58*, 15109–15118. DOI: 10.1021/acs.iecr.9b02679.

(4) Bagheri, A.; Jin, J. Photopolymerization in 3D Printing. *ACS Appl. Polym. Mater.* **2019**, *1*, 593–611. DOI: 10.1021/acsapm.8b00165.

(5) Wilts, E. M.; Pekkanen, A. M.; White, B. T.; Meenakshisundaram, V.; Aduba, D. C.; Williams, C. B.; Long, T. E. Vat Photopolymerization of Charged Monomers: 3D Printing with Supramolecular Interactions. *Polym. Chem.* **2019**, *10*, 1442–1451. DOI: 10.1039/c8py01792a.

(6) Ngo, T. D.; Kashani, A.; Imbalzano, G.; Nguyen, K. T. Q.; Hui, D. Additive Manufacturing (3D Printing): A Review of Materials, Methods, Applications and Challenges. *Compos. Part B Eng.* **2018**, *143*, 172–196. DOI: 10.1016/j.compositesb.2018.02.012.

(7) Ligon, S. C.; Liska, R.; Stampfl, J.; Gurr, M.; Mulhaupt, R. Polymers for 3D Printing and Customized Additive Manufacturing. *Chem. Rev.* **2017,** *117,* 10212-10290. DOI: 10.1021/acs.chemrev.7b00074.

(8) Ding, R.; Du, Y.; Goncalves, R.; Francis, L.; Reineke, T. Sustainable near UV-Curable Acrylates Based on Natural Phenolics for Stereolithography 3D Printing. *Polym. Chem.* **2019**, *10*, 1067. DOI: 10.1039/c8py01652f.

(9) Kim, S. H.; Yeon, Y. K.; Lee, J. M.; Chao, J. R.; Lee, Y. J.; Seo, Y. B.; Sultan, T.; Lee, O. J.; Lee, J. S.; Yoon, S.; Hong, I.; Khang, G.; Lee, S.; Yoo, J. Park, C. Precisely Printable and Biocompatible Silk Fibroin Bioink for Digital Light Processing 3D Printing. *Nat. Commun.* **2018**, *9*, 1620. DOI: 10.1038/s41467-018-03759-y.

(10) Lim, K. S.; Schon, B. S.; Mekhileri, N. V.; Brown, G. C. J.; Chia, C. M.; Prabakar, S.; Hooper, G. J.; Woodfield, T. B. F. New Visible-Light Photoinitiating System for Improved Print Fidelity in Gelatin-Based Bioinks. *ACS Biomater. Sci. Eng.* **2016**, *2* , 1752–1762. DOI: 10.1021/acsbiomaterials.6b00149.

(11) Poldervaart, M. T.; Goversen, B.; Ruijter, M. De; Abbadessa, A.; Melchels, P. W.; Cumhur, F. O.; Dhert, W.; Vermonden, T.; Alblas, J. 3D Bioprinting of Methacrylated Hyaluronic Acid (MeHA) Hydrogel with Intrinsic Osteogenicity. *PLoS One* **2017**, *12*, e0177628. DOI: 10.1371/journal.pone.0177628

(12) Lim, K.; Levato, R.; Costa, P.; Castilho, M.; Alcala-Orozco, C.; van Dorenmalen, K.; Melchels, F.; Gawlitta, D.; Hooper, G.; Malda, J.; Woodfield, T. Bio-Resin for High Resolution Lithography-Based Biofabrication of Complex Cell-Laden Constructs. *Biofabrication* **2018**, *10*, 034101. DOI: 10.1088/1758-5090/aac00c.

(13) Dilla, R. A.; Motta, C. M. M.; Snyder, S. R.; Wilson, J. A.; Wesdemiotis, C.; Becker, M. L. Synthesis and 3D Printing of PEG-Poly(Propylene Fumarate) Diblock and Triblock

Copolymer Hydrogels. *ACS Macro Lett.* **2018**, *7*, 1254–1260. DOI: 10.1021/acsmacrolett.8b00720.
(14) Childers, E. P.; Wang, M. O.; Becker, M. L.; Fisher, J. P.; Dean, D. 3D Printing of Resorbable Poly (Propylene Fumarate) Tissue Engineering Scaffolds. *Mater. Res. Soc.* **2015**, *40*, 119–126. DOI: 10.1557/mrs.2015.2.
(15) Choi, J.; Wicker, R.; Lee, S.; Choi, K.; Ha, C.; Chung, I. Fabrication of 3D Biocompatible / Biodegradable Micro-Scaffolds Using Dynamic Mask Projection Microstereolithography. *J. Mater. Process. Technol.* **2009**, *209*, 5494–5503. DOI: 10.1016/j.jmatprotec.2009.05.004.
(16) Seck, T. M.; Melchels, F. P. W.; Feijen, J.; Grijpma, D. W. Designed Biodegradable Hydrogel Structures Prepared by Stereolithography Using Poly (Ethylene Glycol)/ Poly (D , L -Lactide) -Based Resins. *J. Control. Release* **2010**, *148*, 34–41. DOI: 10.1016/j.jconrel.2010.07.111.
(17) Hiemenz, P. C.; Lodge, T. *Polymer Chemistry*, 2nd ed.; CRC Press: Boca Raton, 2007.
(18) Hinczewski, C.; Corbel, S.; Chartier, T. Ceramic Suspensions Suitable for Stereolithogiaphy. *J. Eur. Ceram. Soc.* **1998**, *18*, 583–590. DOI: 10.1016/S0955-2219(97)00186-6
(19) Sutton, J. T.; Rajan, K.; Harper, D. P.; Chmely, S. C. Lignin-Containing Photoactive Resins for 3D Printing by Stereolithography. *ACS Appl. Mater. Interfaces* **2018**, *10*, 36456–36463. DOI: 10.1021/acsami.8b13031.
(20) Luo, Y.; Le Fer, G.; Dean, D.; Becker, M. L. 3D Printing of Poly(Propylene Fumarate) Oligomers: Evaluation of Resin Viscosity, Printing Characteristics and Mechanical Properties. *Biomacromoles* **2019**, *20*, 1699-1708. DOI: 10.1021/acs.biomac.9b00076.
(21) Seiler, M. Hyperbranched Polymers : Phase Behavior and New Applications in the Field of Chemical Engineering. *Fluid Phase Equilib.* **2006**, *241*, 155–174. DOI: 10.1016/j.fluid.2005.12.042.
(22) Voit, B. I.; Lederer, A. Hyperbranched and Highly Branched Polymer Architectures s Synthetic Strategies and Major Characterization Aspects. **2009**, *109*, 5924–5973. DOI: 10.1021/cr900068q
(23) Reed, R. G.; Feldhoff, R. C.; Clute, O.; Peters, T. Fragments of Bovine Serum Albumin Produced by Limited Proteolysis. Conformation and Ligand Binding. *Biochemistry* **1975**, *14*, 4578–4583. DOI: 10.1021/bi00692a004.
(24) Ueki, T.; Hiragi, Y.; Kataoka, M.; Inoko, Y.; Amemiya, Y.; Izumi, Y.; Tagawa, H.; Muroga, Y. Aggregation of Bovine Serum Albumin Upon Cleavage of Its Disulfide Bonds, Studied by the Time-Resolved Small-Angle X-Ray Scattering Technique with Synchrotron Radiation. *Biophys. Chem. 23*, 115–124. DOI: 10.1016/0301-4622(85)80069-7.
(25) Gauvin, R.; Chen, Y.; Woo, J.; Soman, P.; Zorlutuna, P.; Nichol, J. W.; Bae, H.; Chen, S.; Khademhosseini, A. Biomaterials Microfabrication of Complex Porous Tissue Engineering Scaffolds Using 3D Projection Stereolithography. *Biomaterials* **2012**, *33*, 3824–3834. DOI: 10.1016/j.biomaterials.2012.01.048.
(26) Shirahama, H.; Lee, B. H.; Tan, L. P.; Cho, N. Precise Tuning of Facile One-Pot Gelatin Methacryloyl (GelMA) Synthesis. *Sci. Rep.* **2016**, *6,* 31036. DOI: 10.1038/srep31036.
(27) Adamczyk, M.; Buko, A.; Chen, Y.; Fishpaugh, J. R.; Gebler, J. C.; Johnson, D. D. Characterization of Protein — Hapten Conjugates . 1 . Matrix-Assisted Laser Desorption Ionization Mass Spectrometry of Immuno BSA — Hapten Conjugates and Comparison

with Other. *Bioconjug. Chem.* **1994**, *5,* 631–635. DOI: 10.1021/bc00030a019.
(28) Micsonai, A.; Wien, F.; Kernya, L.; Lee, Y.; Goto, Y.; Réfrégiers, M.; Kardos, J. Accurate Secondary Structure Prediction and Fold Recognition for Circular Dichroism Spectroscopy. *Proc. Natl. Acad. Sci. U. S. A.* **2015**, 3095–3103. DOI: 10.1073/pnas.1500851112.
(29) Micsonai, A.; Wien, F.; Bulyaki, E.; Kun, J.; Eva, M.; Lee, Y.; Goto, Y.; Matthieu, R.; Kardos, J. BeStSel : A Web Server for Accurate Protein Secondary Structure Prediction and Fold Recognition from the Circular Dichroism Spectra Andr As. *Nucleic Acids Res.* **2018**, *46*, 315–322. DOI: 10.1093/nar/gky497.
(30) Ewoldt, R. H.; Johnston, M. T.; Caretta, L. M. *Complex Fluids in Biological Systems*; Spagnolie, S., Ed.; **2015**. DOI: 10.1007/978-1-4939-2065-5_6.
(31) Schwartz, J. J.; Boydston, A. J. Multimaterial Actinic Spatial Control 3D and 4D Printing. *Nat. Commun.* **2019**, *10*, 791. DOI: 10.1038/s41467-019-08639-7.
(32) Bhattacharjee, N.; Parra-cabrera, C.; Kim, Y. T.; Kuo, A. P.; Folch, A. Desktop-Stereolithography 3D-Printing of a Poly (Dimethylsiloxane) -Based Material with Sylgard-184 Properties. *Adv. Mater.* **2018**, *30,* 1800001. DOI: 10.1002/adma.201800001.
(33) Dolinski, N. D.; Page, Z. A.; Callaway, E. B.; Eisenreich, F.; Garcia, R. V; Chavez, R.; Bothman, D. P.; Hecht, S.; Zok, F. W.; Hawker, C. J. Solution Mask Liquid Lithography (SMaLL) for One-Step , Multimaterial 3D Printing. *Adv. Mater.* **2018**, *30,* 1800364. DOI: 10.1002/adma.201800364.
(34) Hegde, M.; Meenakshisundaram, V.; Chartrain, N.; Sekhar, S.; Tafti, D.; Williams, C. B.; Long, T. E. 3D Printing All-Aromatic Polyimides Using Mask-Projection Stereolithography : Processing the Nonprocessable. *Adv. Mater.* **2017**, 29, 1701240. DOI: 10.1002/adma.201701240.
(35) Palaganas, N. B.; Mangadlao, J. D.; Leon, A. C. C. De; Palaganas, J. O.; Pangilinan, K. D.; Lee, Y. J.; Advincula, R. C. 3D Printing of Photocurable Cellulose Nanocrystal Composite for Fabrication of Complex Architectures via Stereolithography. *ACS Appl. Mater. Interfaces* **2017**, *9*, 34314–34324. DOI: 10.1021/acsami.7b09223.
(36) de Beer, M. P. De; Laan, H. L. Van Der; Cole, M. A.; Whelan, R. J.; Burns, M. A.; Scott, T. F. Rapid , Continuous Additive Manufacturing by Volumetric Polymerization Inhibition Patterning. *Sci. Adv.* **2019**, *5*, eaau8723. DOI: 10.1126/sciadv.aau8723
(37) Zhu, W.; Tringale, K. R.; Woller, S. A.; You, S.; Johnson, S.; Shen, H.; Schimelman, J.; Whitney, M.; Steinauer, J.; Xu, W.; Yaksh, T.; Nguyen, Q.; Chen, S. Rapid Continuous 3D Printing of Customizable Peripheral Nerve Guidance Conduits. *Mater. Today* **2018**, *21*, 951–959. DOI: 10.1016/j.mattod.2018.04.001.
(38) Torres, O. B.; Jalah, R.; Rice, K. C.; Li, F.; Antoline, J. F. G.; Iyer, M.; Jacobson, A.; Boutaghou, M.; Alving, C.; Matyas, G. Characterization and Optimization of Heroin Hapten-BSA Conjugates : Method Development for the Synthesis of Reproducible Hapten-Based Vaccines. *Anal. Bioanal. Chem.* **2014**, *406*, 5927–5937. DOI: 10.1007/s00216-014-8035-x.
(39) Mondschein, R.; Kanitkar, A.; Williams, C. B., Verbridge, S. S.; Long, T. E. Polymer Structure-Property Requirements for Stereolithographic 3Dprinting of Soft Tissue Engineering Scaffolds. *Biomaterials* **2017**, *140*, 170–188. DOI: 10.1016/j.biomaterials.2017.06.005
(40) Schüller-Ravoo, S.; Teixeira, S. M.; Feijen, J.; Grijpma, D. W.; Poot, A. A. Flexible and Elastic Scaffolds for Cartilage Tissue Engineering Prepared by Stereolithography Using

Poly(Trimethylene Carbonate)-Based Resins. *Macromol. Biosci.* **2013**, *13*, 1711–1719. DOI: 10.1002/mabi.201300399.
(41) Mezger, T. G. *The Rheology Handbook*, 4th ed. Vincentz Network. **2014**
(42) ASTM Standard D4473, 2008 (2016), "Dynamic Mechanical Properties: Cure Behavior," ASTM International, West Conshohocken, PA, 2003 DOI 10.1520/D4473-08R16, Www.Astm.Org. **2016**.
(43) Melchels, F. P. W.; Feijen, J.; Grijpma, D. W. A Review on Stereolithography and Its Applications in Biomedical Engineering. *Biomaterials* **2010**, *31*, 6121–6130. DOI: 10.1016/j.biomaterials.2010.04.050.
(44) Gosal, W. S.; Ross-murphy, S. B. Globular Protein Gelation. *Curr. Opin. Colloid Interface Sci.* **2000**, *5*, 188–194. DOI: 10.1016/S1359-0294(00)00057-1
(45) Chen, J.; Ma, X.; Dong, Q.; Song, D.; Hargrove, D.; Vora, S.; Ma, A.; Lu, X.; Lei, Y. Self-Healing of Thermally-Induced, Biocompatible and Biodegradable Protein Hydrogel. *RSC Adv.* **2016**, *6,* 56183–56192. DOI: 10.1039/c6ra11239k.
(46) Clark, A. H.; Kavanagh, G. M.; Ross-murphy, S. B. Globular Protein Gelation-Theory and Experiment. *Food Hydrocoll.* **2001**, *15,* 383-400. DOI: 10.1016/S0268-005X(01)00042-X
(47) Baler, K.; Michael, R.; Szleifer, I.; Ameer, G. A. Albumin Hydrogels Formed by Electrostatically Triggered Self- Assembly and Their Drug Delivery Capability. *Biomacromolecules* **2014**, *15,* 3625–3633. DOI: 10.1021/bm500883h.
(48) Murayama, K.; Tomida, M. Heat-Induced Secondary Structure and Conformation Change of Bovine Serum Albumin Investigated by Fourier Transform Infrared Spectroscopy. *Biochemistry* **2004**, *43*, 11526–11532. DOI: 10.1021/bi0489154.
(49) Scott, E. A.; Nichols, M. D.; Cordova, L. H.; George, B. J.; Jun, Y. S.; Elbert, D. L. Protein Adsorption and Cell Adhesion on Nanoscale Bioactive Coatings Formed from Poly(Ethylene Glycol) and Albumin Microgels. *Biomaterials* **2008**, *29*, 4481–4493. DOI: 10.1016/j.biomaterials.2008.08.003.
(50) Dikovsky, D.; Bianco-Peled, H.; Seliktar, D. The Effect of Structural Alterations of PEG-Fibrinogen Hydrogel Scaffolds on 3-D Cellular Morphology and Cellular Migration. *Biomaterials* **2006**, *27*, 1496–1506. DOI: 10.1016/j.biomaterials.2005.09.038.
(51) Klein, F.; Richter, B.; Striebel, T.; Franz, C. M.; Freymann, G. Von; Wegener, M.; Bastmeyer, M. Two-Component Polymer Scaffolds for Controlled Three-Dimensional Cell Culture. *Adv. Mater.* **2011**, *23*, 1341–1345. DOI: 10.1002/adma.201004060.

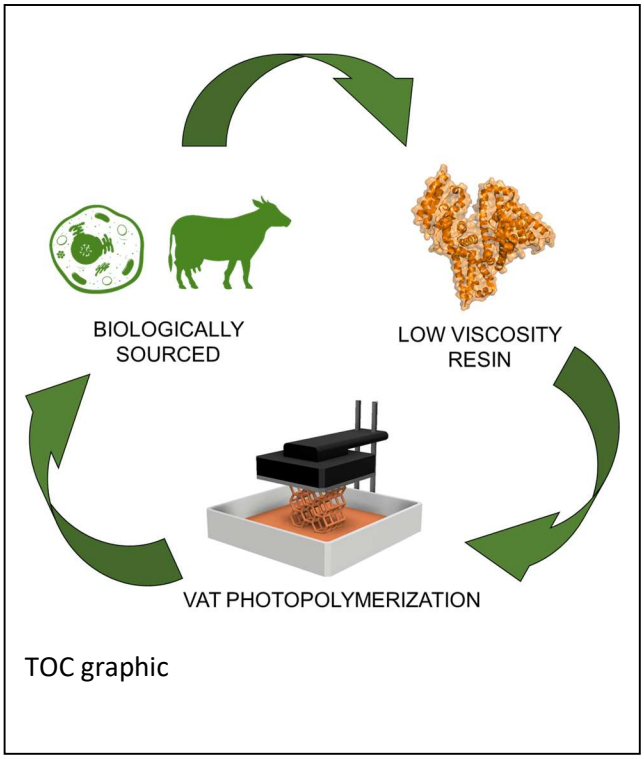
BIOLOGICALLY
SOURCED
LOW VISCOSITY
RESIN
VAT PHOTOPOLYMERIZATION

TOC graphic